Published online October 26, 2004

Nucleic Acids Research, 2004, Vol. 32, No. 19 ***e144***
doi:10.1093/nar/gnh145

Reversibly switchable DNA nanocompartment on surfaces

Youdong Mao[1,3], Chunxiong Luo[1,3], Wei Deng[6], Guangyin Jin[2], Xiaomei Yu[5], Zhaohui Zhang[3], Qi Ouyang[1,4,*], Runsheng Chen[6] and Dapeng Yu[2]

[1]Laboratory for Biotechnology, [2]Laboratory for Nanofabrication, [3]Department of Physics, [4]Center for Theoretical Biology and [5]Institute of Microelectronics, Peking University, Beijing 100871, China and [6]Laboratory for Bioinformatics, Institute of Biophysics, Chinese Academy of Sciences, Beijing 100101, China

Received July 27, 2004; Revised September 21, 2004; Accepted October 6, 2004

ABSTRACT

Biological macromolecules have been used to fabricate many nanostructures, biodevices and biomimetics because of their physical and chemical properties. But dynamic nanostructure and biomachinery that depend on collective behavior of biomolecules have not been demonstrated. Here, we report the design of DNA nanocompartments on surfaces that exhibit reversible changes in molecular mechanical properties. Such molecular nanocompartments are used to encage molecules, switched by the collective effect of Watson–Crick base-pairing interactions. This effect is used to perform molecular recognition. Furthermore, we found that 'fuel' strands with single-base variation cannot afford an efficient closing of nanocompartments, which allows highly sensitive label-free DNA array detection. Our results suggest that DNA nanocompartments can be used as building blocks for complex biomaterials because its core functions are independent of substrates and mediators.

INTRODUCTION

Biological macromolecules with amazing polymorphism have shown their ability in molecular machinery (1–3), devices (4,5) and computation (6). In principle, such ability could incorporate the molecular 'bottom-up' approach (7–9), leading to a nanostructure with potential for molecular device applications. Building blocks with properties independent of substrates or mediators are undoubtedly significant to developing a functional and complex nanosystem. Mechanical behavior of single or few biomolecules has been well-demonstrated (1–3). It is difficult, however, to use these molecular machines as the building blocks of a complex nanosystem. The implementation of a biomolecular mechanical device that depends on the collective behavior of molecules on a surface, which in principle would provide a kind of building blocks with the above-mentioned feature, remains challenging. While a recent study reports the design of a reversibly switching surface (10), the study of dynamic collective behavior is still in its early age. Efforts to engineer a surface switched by biomolecular mechanical properties may lead to new breakthroughs in nanomaterial researches.

Recently, we found that specially designed DNA array can form a molecular cage on surfaces. This molecular cage is switchable due to allosteric transformation driven by the collective hybridization of DNA. We named it 'active DNA nanocompartment (ADNC)'. A typical DNA motif designed to fabricate ADNC comprises two contiguous elements (inset to Figure 1A): a double-stranded DNA (dsDNA) whose array is responsible for a compact membrane (Figure 1A, right) and a single-stranded DNA (ssDNA) serving as skeleton supporting the dsDNA membrane, which is terminated on its 5′ end by a surface linker such as an alkanethiol group that can immobilize DNA on gold surface with a sulfur–gold bond (11–16). Because the diameter of ssDNA is much smaller than that of dsDNA, a compartment with designable effective height (h_{eff}, 5–50 nm, commensurate with the length of ssDNA skeleton) can form between the dsDNA membrane and substrate surface.

Here, we report some basic properties of ADNC, and then explore its implication in practical utility. First, we define the basic structure by atomic force microscopy (AFM) approach. We then show that ADNC switching is controllable, and the experiments are repeated using different indicators and substrates. Furthermore, we find that target sequences with single-base variation cannot afford an efficient closing of ADNC. ADNC with triple state is also introduced here.

MATERIALS AND METHODS

Preparation of ADNC

The gold substrate was cleaned in a H_2SO_4:H_2O_2 solution (7:3), or prepared by gold vapor-deposition on mica, and annealed using a high-purity hydrogen/air flame to yield Au(111) surfaces. The prepared gold substrates were incubated in 0.5 μM thiol-terminated dsDNA solution (Tris–HCl buffer, pH 7.8, 1 mM $MgCl_2$) for 12–24 h at 4°C. The control samples with lower coverage of DNA motifs were

*To whom correspondence should be addressed. Tel: +86 10 62756943; Fax: +86 10 62751615; Email: qi@pku.edu.cn
Correspondence may also be addressed to Youdong Mao. Tel: +86 10 62528034; Fax: +86 10 62751615; Email: jackmao@water.pku.edu.cn

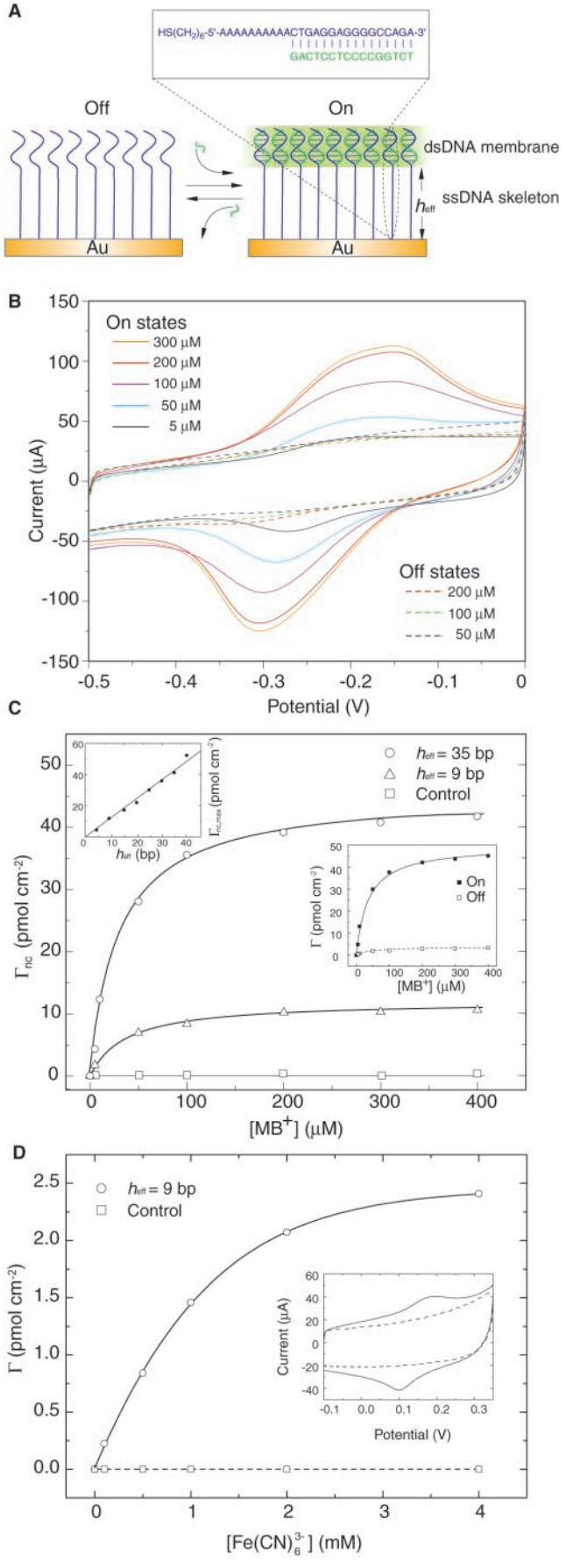

prepared either by shortening the duration of incubation to 1 min (11,17) or by decreasing the DNA concentration to 50 nM.

AFM imaging

All images were taken in air using Digital Instruments Nanoscope IIIa (CA, USA) and SII SPI3800N (Japan) with tapping mode. Most images were leveled using a first-order plane fit to remove sample tilt.

Hybridization, electrochemical measurement and analysis of surface concentration Γ

To use the ADNC to encage methylene blue (MB^+), the devices were initially set to the off state (see Figure 1A) and put into the hybridization solution (Tris–HCl buffer, pH 7.8, 0.1 M NaCl, 1 mM $MgCl_2$) containing both the 'fuel' strands and MB^+. Hybridization lasted for at least 2–3 h. Measurement of the surface density of MB^+ (Γ) was conducted in an electrochemical cell (sodium phosphate buffer, pH 7, without any electroactive species) with three-electrode configuration (functionalized gold working electrode, Pt auxiliary electrode, and ultralow leakage Ag/AgCl/3 M KCl reference electrode) based on CHI660A Electrochemical Workstation (CH Instrument, Austin, TX). Before each measurement, the device was separated from the hybridization solution, and rinsed with 1 M sodium salt in Tris–HCl buffer (pH 7.8) to remove the reversibly adsorbed but not encaged MB^+. Salt-washing for 30–60 s was used in the plots of the isotherms (Figures 1B, C and 5) and 15 s in the plots of $\Gamma_{nc}(t)$ (Figure 3).

The surface concentration (Γ) of the reporters confined on surfaces should be $\Gamma = \Gamma_{nc} + \Gamma_{dsDNA} + \Gamma_{ads}$, where Γ_{nc}, Γ_{dsDNA} and Γ_{ads} are, respectively, the surface concentrations of indicators encaged in the closed ADNC, intercalated into dsDNA membrane (14,18–20) and adsorbed irreversibly to the bottom of the nanocompartment. When $h_{eff} > 5$ nm, Γ_{dsDNA} is no longer addressable due to the low efficiency of electron transfer through adenine and thymine bases (21,22) (see Supplementary Material for evidence). Thus, for an ADNC with $h_{eff} > 5$ nm, the detectable indicators trapped in the ADNC

Figure 1. (**A**) Schematic drawing of a dual-state ADNC. By adding or removing 'fuel' strands (green), the ADNC can be switched between on (right) and off (left) state. Inset, a typical sequence used to fabricate ADNC. The green 'fuel' strand is a segment of human p53 gene containing one site of most frequent mutation. (**B**) Original cyclic voltammograms of ADNC for the on and off states with different $[MB^+]$ configurations. Insets show the $[MB^+]$ corresponding to each colorized curve. Scan rate = 4 V s^{-1}. Sample interval = 0.001 V. (**C**) Isotherms for MB^+ in an on-state ADNC at room temperature. Γ_{nc} is the difference between Γ measured in the on state and the off state. (Left inset) The relationship between $\Gamma_{nc,max}$ and h_{eff}. The slope of the Γ_{nc}–h_{eff} curve (~10 mM) represents the saturation concentration of MB^+ in the closed ADNC. (Right inset) Binding isotherms of Γ for MB^+ in an ADNC (h_{eff} = 35 bp) with on and off states respectively. The on/off ratio of the amount concentration (Γ) for MB^+ confined ranges from 10 to 18, whereas the ratio for $[Fe(CN)_6]^{3-}$ almost reaches >100. Control experiments (open square) were based on the samples with a low density of the same DNA motifs (~1.6 × 10^{12} molecules cm^{-2}). (**D**) Isotherms for $[Fe(CN)_6]^{3-}$ in an on-state ADNC at room temperature (h_{eff} = 9 bp). Inset shows typical cyclic voltammogram on an on-state ADNC encaging $[Fe(CN)_6]^{3-}$ ($[Fe(CN)_6^{3-}]$ = 2 mM). Scan rate = 1 V s^{-1}. Dashed line shows the control experiments performed on the ADNC that was hybridized with single-base mismatches.

interface should be

$$\Gamma = \begin{cases} \Gamma_{nc} + \Gamma_{ads} & \text{for the on state} \\ \Gamma_{ads} & \text{for the off state.} \end{cases} \quad \mathbf{1}$$

When we use cyclic voltammetry (CV) to address the redox indicators confined in ADNC interfaces, the peak current in the resulting voltammogram (the difference between the maximum current and baseline current) is given by (23):

$$i_p = \frac{n^2F^2}{4RT} v \cdot A \cdot \Gamma. \quad \mathbf{2}$$

Here n is the number of electrons per molecule for a redox reaction, F the Faraday constant, R the gas constant, T the temperature, v the scan rate of potential and A the electrode area. This equation provides a means to determine Γ approximately. We also use the chronocoulometry (CC) (11) and AC voltammetry (14) to perform the measurement of Γ, which give a consistent result. The optimal frequency used in AC voltammetry for MB^+ addressing was 200 Hz. A = 100 μm^2, 0.03 cm^2, 0.18 cm^2. Scan rate of CV was 4 V s^{-1} for the measurements.

Other oligonucleotide sequences used in the experiments of Figure 1 are as follows: 5′-$(A)_9$CTGAGGAGG-3′; 5′-$(A)_{10}$CTGAGGAGGGGCCAGA-3′; 5′-$(A)_{20}$GCCTTAACTGTAGTACTGGTGAAATTGCTG-3′.

Determining the DNA density

Two methods were used to determine the density of DNA self-assembled. The first method is a direct measurement on the high resolution of AFM images (inset to Figure 2C). The second method is to modify the complementary strands with fluorescein ($C_{20}H_{10}Na_2O_5$; Sigma) before the self-assembly procedure. After self-assembly, the complementary strands could be washed away from surfaces by heating denaturation. The fluorescent light intensity could be measured by Inverse Fluorescence Microscope IX70 (Olympus, Japan) with cooling CCD (Princeton Instrument, TX, USA). According to the detected fluorescent intensity, we could calculate the amount of DNA molecules immobilized on the surface and then deduct the DNA density by dividing the amount of DNA by the surface area. The two methods give the results of 5.4 ± 0.8 × 10^{12} molecules cm^{-2} and 5.0 ± 1.0 × 10^{12} molecules cm^{-2}, respectively, which are consistent within the error bar.

Allele-specific oligonucleotide (ASO) probe sequences

Hybridization probe sequences employed for the ASOs are listed as follows. Each ASO has a 15 nucleotide poly dT spacer sequence at the 5′ end and an alkanethiol group (HS-$(CH_2)_6$-) at the 5′ terminus.

M168 mutant	5′-GGAGGTGAGTTGCTAGC-3′
Wild type	5′-GGAGGTGAGTCGCTAGC-3′
M175 mutant	5′-CTCACTTCTCAAGAATGAATG-3′
Wild type	5′-CTCACTTCTCTTCTCAAGAAT-3′
M203 mutant	5′-CTGCGCACGATTTCA-3′
Wild type	5′-CTGCGCAGGATTTCA-3′
M213 mutant	5′-TAAGAAGTCACGTAACGAGAT-3′

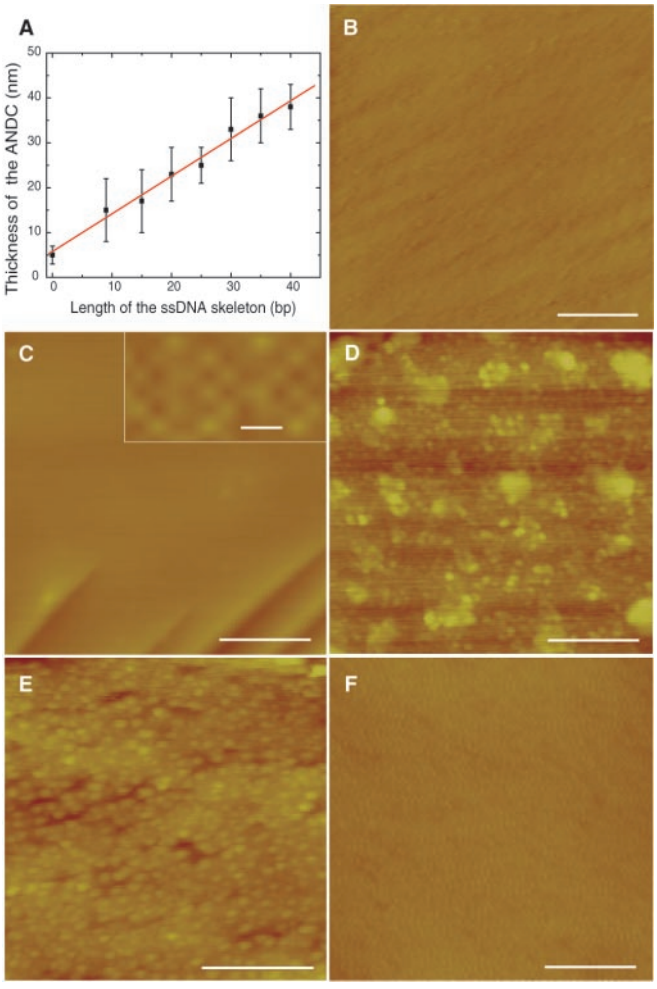

Figure 2. AFM measurements show the topographies of ADNC on Au(111) surface. (**A**) The thickness, measured on the edge of the ADNC, as a function of the length of the ssDNA skeleton. (**B**) The blank gold surface as a control experiment. (**C**) The initial on state of the ADNC. The inset shows a crystalline lattice with the periodicity of 4.0 ± 0.5 nm, which was found on well-formed dsDNA membrane. The diameter of one dsDNA molecule can be directly measured to be ~2 nm, proving the image is the top view of dsDNA. (**D**) The off state of the ADNC after denaturation, which shows local aggregation of immobilized ssDNA. (**E**) Insufficient rehybridization, which offers a medium inhomogeneous array to the extent between (D) and (F). (**F**) The on state of the device after sufficient rehybridization. Height scales are 50 nm in (C), 10 nm in (B) and (D)–(F), and 5 nm in the inset to (C). Scale bars are 25 nm in (B), 250 nm in (C)–(F) and 5 nm in the inset to (C).

Wild type	5′-TAAGAAGTCATGTAACGAGAT-3′
M216 mutant	5′-AAAGAAATGTAATATTCAACAG-3′
Wild type	5′-AAGAAATGTAACATTCAACAG-3′
M217 mutant	5′-GGTGACACCAACTCTTCAG-3′
Wild type	5′-GGTGACACAAACTCTTCAG-3′

The design of these ASO sequences was under consideration for duplex stability, discrimination between matches and mismatches, and uniformity of melting temperature for different strands. All the listed ASO sequences have melting temperatures in a small range of 47–49°C, with mismatches placed near the center of the sequences, which meet the need for the optimization of discrimination between matches and mismatches (17,24).

Genomic DNA amplification

Human genomic DNAs were acquired from male blood samples from a recent survey of Chinese ethnical minorities' Y chromosome single nucleotide polymorphism (SNP) (unpublished data). Five segments, 473, 444, 503, 409 and 1018 bp in length, were amplified by PCR, using the following primers: M168: 5′-agtttgaggtagaatactgtttgct-3′, reverse 5′-aatctcataggtctctgactgttc-3′; M175: 5′-ttgagcaagaaaaatagtaccca-3′, reverse 5′-ctccattcttaactatctcaggga-3′; M203: 5′-gagtgccaagcctgaggatga-3′, reverse 5′-tccttggcagccgctgaggag-3′; M213: 5′-tataatcaagttaccaattactggc-3′, reverse 5′-ttttgtaacattgaatggcaaa-3′; M216 and M217: 5′-ctcaaccagtttttatgaagctag-3′, reverse 5′-acctgttgaatgttacatttcttt-3′; PCR was performed in a thermocycler, PE 2400 (Applied Biosystems, Foster City, CA), to amplify the SNPs containing sequence tagged site (STS) sequences. The 15 µl reaction solution contained 1× standard PCR buffer, 2 µM of each primer, 200 µM dNTPs, 0.5 U *Taq* DNA polymerase and 50 ng genomic DNA. The thermocycle employed was: 94°C for 2 min, 40 cycles, each of which consists of 15 s at 94°C, 15 s at 56°C and 40 s at 72°C, and a 2 min final extension at 72°C. PCR products were purified with wizard PCR Preps DNA Purification System (Promega) and used as templates in amplification and sequencing reaction of ssDNAs. The linear amplification contained the same reaction solution except: 2 µM one end primer that primed the strand complement to the corresponding ASO sequence and 10 ng of the template. The thermocycle employed was: 94°C for 2 min, 20 cycles, each of which consists of 15 s at 94°C and 2 min at 60°C. Polymorphism types were also proved by Big-Dye terminator sequencing on a PE Biosystem 3700 sequencer (Applied Biosystems, Foster City, CA).

SNPs analysis

The sensor chip was made simply by packing 10 µM gold electrodes into an array as the layout shown in Figure 4A. Gold microelectrodes employed are available at CH Instruments (Austin, TX). ASO modification was performed as described above. Hybridization was carried out in 10 µl of a 500 pM solution of the genomic DNA dissolved in 20 mM Tris–HCl buffer (pH 8.0) containing 100 mM NaCl, 1 mM $MgCl_2$ and 10 µM MB^+. The functionalized surface of the sensor chip was incubated in hybridization buffer for 14 h at 38°C in a closed tube over water. After hybridization, the sensor chip was washed with Tris–HCl buffer containing 1 M NaCl for 30 s. Electrochemical CV detection was carried out as described above. After one round of experiment, the chip was washed by urea to remove the surface-bound targets and then stored in Tris–HCl buffer at 4°C, which made it reusable in other SNPs analysis experiments.

RESULTS AND DISCUSSION

Rational design in interfacial engineering

A typical DNA motif is shown in inset to Figure 1A. The 'fuel' strand (green in inset to Figure 1A), used to switch the DNA compartment, is selected from the human *p53* gene, one of the frequently mutated residues. A conformational transition between 'on' and 'off' states of ADNC requires synergistic molecular reorganization of ordered DNA motif. In principle, the formation of ADNC depends on three conditions: (i) whether the dsDNA portion can be densely packed into a relatively impermeable membrane; (ii) whether the dsDNA membrane can be formed reversibly by *in situ* hybridization; and (iii) whether the nanocompartment can continuously span across a sufficient area.

Dense molecular packing of ssDNA self-assembled monolayer (SAM) and strong interactions between the sugar–phosphate backbones of ssDNA restrict molecular hybridization (11–17). However, 100% hybridization efficiency is achievable if the density is in a proper range (supposing that other factors are fixed) (11,12,17). Theoretical expectation of the optimum density for ADNC formation is $5 \pm 2 \times 10^{12}$ molecules cm^{-2}; lower or higher density will notably result in the failure of its formation. To establish sufficient spatial freedom for molecular hybridization, we have ssDNA capped by a helical dsDNA segment (green in Figure 1A) before the ssDNA motif self-assembled on the surface. This results in a SAM that is densely packed with respect to the space-filling helical cap, but shows low-density packing with respect to the ssDNA skeleton. Subsequent removal of the space-filling helical cap by denaturation establishes an appropriate density for SAM, which is measured to be $5.4 \pm 0.8 \times 10^{12}$ molecules cm^{-2}, within the optimum density range. Similar methods to control self-assembly density can be found in other reports (10,18).

Experimental definition on the basic structure of ADNC

To experimentally define the basic nanostructure of ADNC, we characterized the surface of the ADNC film using AFM. We investigated the changes in thickness of ADNC with different base numbers of its ssDNA skeleton by measuring the profiles of the ADNC film at its edge (see Supplementary Material). The results presented in Figure 2A show that the thickness of ADNC increases linearly with elongation of the ssDNA skeleton. The slope of the curve is $\sim 0.8 \pm 0.2$ nm per base. Because the tapping mode of AFM measurement often gives a systematic error in *z*-direction, the data is slightly larger than that for the measured object. If we consider the low limit of the error bar and the systematic error in measuring, the data roughly agree with previously reported measurements (19,20). This indicates that the immobilized DNA motifs are oriented perpendicular to the gold surface, which is consistent with the results presented in the literatures (12–14).

Figure 2C–F shows the topographic observations of the same ADNC sample at different conditions. The topographies of the initial 'on' state of the freshly prepared device and subsequent 'off' state, achieved by denaturation, are shown in Figure 2C and D, respectively. The image taken after sufficient rehybridization (Figure 2F) provides a reformed homogeneous array of dsDNA (compared with Figure 2D and E), verifying that the switching of ADNC is reversible. These direct observations agree that high hybridization efficiency ($\sim$100%) was yielded in our experiments (12,17).

To confirm the topographic changes of DNA film observed by AFM, we conducted more experiments on the same sample for a different state. Two evidences in these experiments could convince us that the results observed in Figure 2 are not from AFM tip effect or surface artifact. First, we observed

the lay-down phase on the same sample, which proved that the DNA film that we observed is real. Second, in the same performance of the experiments, we observed an image very similar to Figure 2D. The repeated observations in the different state of the same sample thus proved that the whole observations are reliable. For the detailed discussions and experiments see Supplementary Material.

Surface defects, mostly pinholes, inevitably prevent a perfect ADNC from spanning across a very broad area, and thus are prone to damage the ADNC performance. We have electrochemically evaluated the overall effect of the pinholes on the ADNC film. The results show that the diffusion of redox reporters through the pinholes can be safely neglected on a macroscopic scale (see Supplementary Material). We thus have clarified the three issues raised above and shown a well-defined nanostructure of ADNC.

Molecular encaging effect

Since ADNC is reversibly switchable, it should be able to encage molecules with suitable size. We name this phenomenon molecular encaging effect. To examine this effect, we used ADNC to encage certain electroactive species. Redox reactions of these species near the gold surface allow us to address it by electrochemical methods (14,23). MB^+, a phenothiazinium dye (25–27), and ferricyanide anions (28) ($[Fe(CN)_6]^{3-}$) were chosen as redox reporters, for they are impermeable through the dsDNA membrane of the ADNC. The devices were initially set to the 'off' state and exposed to a hybridization solution containing both the 'fuel' strands and the reporters for at least 2–3 h (see Methods). Once the closed ADNC entrapped some reporters, the Γ_{nc} of the encaged reporters could be determined by CV (Figure 1B, see Methods). Figure 1C and D give the isotherms of the molecular encaging effect for MB^+ and $[Fe(CN)_6]^{3-}$ respectively. Control experiments show that high density of immobilized ssDNA ($>8 \times 10^{12}$ molecules cm^{-2}) would notably decrease the 'on/off' ratio to 1∼2, due to the low hybridization efficiency and the failure of ADNC formation, and that low density ($<2 \times 10^{12}$ molecules cm^{-2}) results in the vanishing of Γ_{nc}. All these isotherms fit well to the Langmuir model (23): $x/\Gamma_{nc} = (1/\Gamma_{nc,max})x + (1/K\Gamma_{nc,max})$, where x is the concentration of the reporter and K is the association constant per site (11,14). The isotherms at different h_{eff} for MB^+ (Figure 1C) give the same K value, showing that single-site binding mode dominates in interactions between ADNC and reporters. While MB^+ obtained $K = (3.0 \pm 0.2) \times 10^4\ M^{-1}$, $[Fe(CN)_6]^{3-}$ obtained $K = (0.9 \pm 0.1) \times 10^3\ M^{-1}$. The difference demonstrates that the electronegativity of $[Fe(CN)_6]^{3-}$ prominently diminished the capacity of ADNC.

The linear relationship between the saturation of Γ_{nc} ($\Gamma_{nc,max}$) and h_{eff} shown in the left inset to Figure 1C demonstrates that the number of encaging sites is proportional to the length of the ssDNA skeleton, providing experimental evidence that the closed ADNC can be considered as a container. The saturation concentration of MB^+ in the closed ADNC is several orders of magnitude higher than $[MB^+]$ in external solution, but is in the same order of magnitude as the concentration of the negative charges provided by ssDNA skeletons (∼50 mM). This suggests that the electrostatic interactions between the negatively charged sugar–phosphate backbone of ssDNA skeleton and the MB^+ cations caused MB^+ to fill up the space of the ADNC. The electrostatic interaction is strongly affected by the ionic strength of the operation solution (11,29,30). We observed that increasing $[Na^+]$ could decrease Γ_{nc} due to the competition between Na^+ and MB^+. At $[Na^+] = 0.5$ M, no encaging effect was observed even using high $[MB^+]$ (0.5 mM). In contrast to MB^+, the saturation concentration of the encaged $[Fe(CN)_6]^{3-}$ (∼10 mM) is at the same order as the concentration of $[Fe(CN)_6]^{3-}$ in the external solution. These results suggest that the capacity of ADNC is determined by the interaction between the encaged species and ADNC backbones, and that the molecular encaging effect is a general property of ADNC.

To further verify the generality of ADNC properties, we also constructed ADNC on a SiO_2 substrate and used fluorescein ($C_{20}H_{10}Na_2O_5$) as optical reporters. Because fluorescein molecules are impermeable through the dsDNA membrane of ADNC, they can be encaged by the ADNC on SiO_2 substrate. Our experimental result by fluorescent microscopy shows similar behavior compared to $[Fe(CN)_6]^{3-}$ and MB^+ (see Supplementary Material). In addition, some DNA motifs with different base numbers in dsDNA membrane, ranging from 9 to 30, are also used to validate the molecular encaging effect (see Methods).

Single-base mismatch detection using ADNC switching

Although we have used perfectly complementary strands as 'fuel' molecules to switch ADNC, it remains unclear whether strands with base mismatches could also serve the same purpose. To examine this question further, we designed a series of experiments to evaluate discrimination of the complementary pair, G:C, from the three single-base mismatches, G:X (X = A, T, G), which is the point mutation site in the human *p53* gene. Typical performance is shown in Figure 3. Using the encaged species as hybridization indicators greatly sharpens the melting profiles for the perfectly complementary targets, and flattens denaturation profiles for the strands with a wobble mismatch. The flattening of the thermal-denaturation curve for mismatches was attributed to the low efficiency of hybridization for mismatches, which was measured to be <50% by quartz crystal microbalance (15). It is comprehensible that when the hybridization efficiency is <50%, the dsDNA film could not form an impermeable membrane. The observation shows that single-base mismatched strands are incapable of closing ADNC on surfaces.

While the fluorescence-labeling-based system has 2.6:1 selectivity at its optimum stringency temperature (42°C), ADNC-based system increases this selectivity to ∼100:1 at a temperature ranging from 10 to 45°C. The improved selectivity in the assay results from the switching of ADNC that depends on a fully collective hybridization. Since two kinds of substrates (gold, SiO_2) and three kinds of indicators (MB^+, $[Fe(CN)_6]^{3-}$, fluorescein $C_{20}H_{10}Na_2O_5$) used in these investigations show consistent results, we conclude that the molecular recognition property of ADNC between matches and mismatches is independent of substrates and indicators. Different realization and implementation of ADNC, however, would reasonably result in a different selectivity and sensitivity. These results suggest that ADNC provides a novel approach to sequence-specific recognition of DNA.

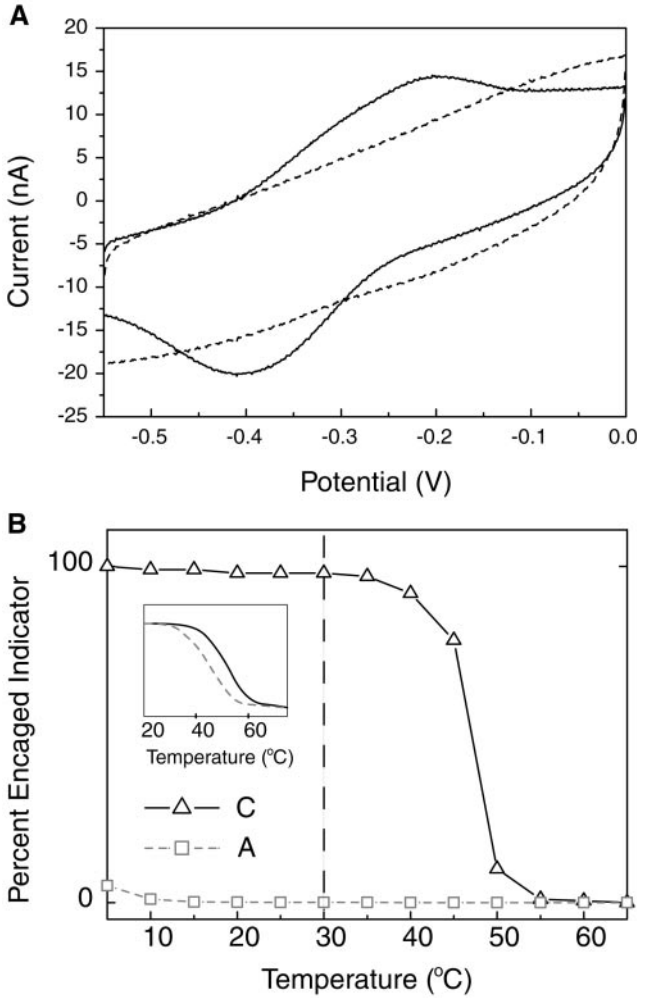

Figure 3. Performance comparison between perfect targets and single mismatches. A typical ADNC motif used in these tests is described in Figure 1A. The corresponding target oligonucleotide has a wobble base represented by X: 5′-TCTGGCCXCTCCTCAG-3′, which is one of the frequent mutations in the human *p53* gene. X = C for the perfectly complementary target. X = A, G or T for the single-base mismatched target. 50 amol of targets are used in the experiments. (**A**) Typical cyclic voltammograms of an ADNC system with 10 μm diameter for the wild type target (solid line) and the single mismatch (dashed line) measured at 25°C, using the encaged molecule as hybridization indicator. (**B**) Dissociation of target from the surface of this ADNC system. Black curves describe DNA duplex thermal-denaturation curve for the perfectly complementary oligonucleotide (X = C), and gray dashed curves for the strand with a wobble mismatch (X = A). The intercepts at the vertical dotted line allow one to estimate the expected ratio of encaged indicator at complementary and mismatched array elements and thus are an estimate of the expected selectivity of sequence identification for ADNC-based gene chips. (Inset) Thermal-denaturation curve monitored by fluorescence-labeling for the perfectly matched DNA (X = C) and the one with a wobble mismatch (X = A). The separation of the two thermal-denaturation curves is therefore enhanced >10-folds as compared with that obtained from an analogous system based on labeling methods.

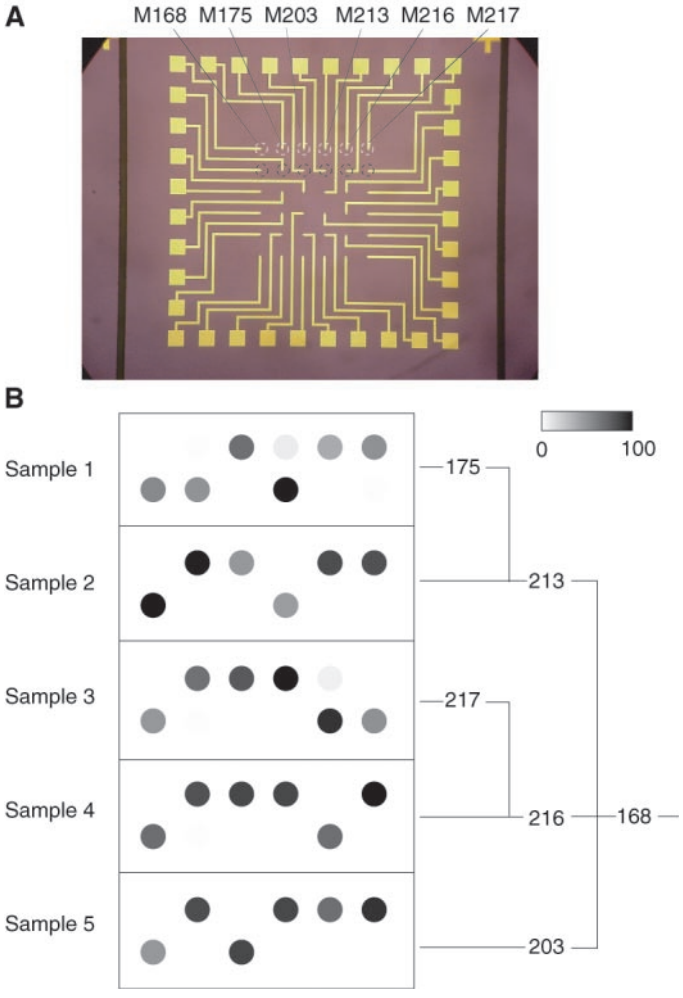

Figure 4. (**A**) Photography of the electronic chip incorporated with ADNC. The detection spot site, marked by dashed-line circles, is a $10 \times 10\ \mu m^2$ square. The connection lines are covered by photoresist. The white-marked spots are activated with ASOs corresponding to the normal allele; the black-marked ones with ASOs corresponding to the mutant allele. Column number M168, M175, M203, M213, M216 and M217 refer to the ASOs employed as given in Experimental protocol. (**B**) Visualized electrochemical data obtained from sensor chips hybridized with single-stranded PCR products. The signal from the saturation of encaged indicators is set as 100; and all data is then normalized to the range of 0–100 for the convenience of visualized computer drawing. The layout of the surface-bound ASOs is shown in (A). Right tree displays parsimony phylogeny of human NRY chromosome biallelic variation. Tree is rooted with respect to non-human primate sequences.

SNPs identification based on electronic sensor chips incorporated with ADNC

We have shown that the ADNC-based system can detect single mutations in a short piece of oligonucleotide; the next natural step is using it as a sensor to discriminate mutations in real samples. The test system consists of six unique event polymorphisms, associated with the non-recombining portion of Y-chromosome (NRY), which are biallelic variations reflecting the microevolutionary trajectory of modern human genetic diversification (31,32). One of the six polymorphic sites is a five-base deletion in a mutant allele, named M175; and the others are single-base variations, named M168, M203, M213, M216 and M217, respectively. The phylogenetic tree of the six NRY polymorphisms is shown to the right of Figure 4B, which was deduced from established knowledge (31,32). We designed twelve ASOs as probes of the SNPs analysis. Sequences of the ASOs are given in the Methods section. Six of the ASO probes correspond to ancestral type sequences at the polymorphic site, and six to the mutant sequences. The ASO probes were arranged in a 2 × 6 array

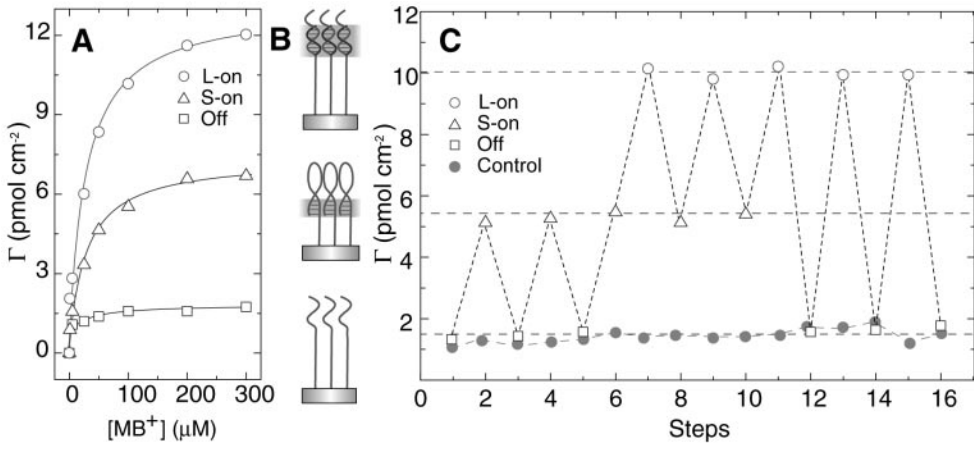

Figure 5. (**A**) Γ isotherms for MB^+ in a triple-state ADNC. A cross-sectional sequence used is 5′-AAAAGCACGCTGAGGAGGGGCCAGACGTGC-3′. The underlined bases are stem sequences. Solid lines are the fits from Langmuir isotherm. For the s-on state, h_{eff} = 5.9 nm. For the l-on state, h_{eff} = 12.4 nm. The measured ratio of Γ_{nc}(l-on)/Γ_{nc}(s-on) (∼2.2) is consistent with the h_{eff} (l-on)/h_{eff}(s-on) (= 2.1), confirming the linear relationship between Γ_{nc} and h_{eff}. (**B**) Schematic drawing of a triple-state ADNC: the l-on state (top), the s-on state (middle) and the off state (bottom). (**C**) Cyclic switching of the triple-state ADNC. [MB^+] = 100 μM. Control experiments (open circle) were based on the samples with a low density of the same DNA motifs (∼1.6×10^{12} molecules cm^{-2}).

of electronic sensors according to the layout shown in Figure 4A, with 10 μm diameter for each spot. Non-labeled single-stranded target DNAs were prepared from genomic DNAs of five male individuals from different haplotypes. The targets belonging to the same individuals were all placed in one mixture sample. Thus, one hybridization experiment gives all the allele states for an individual and his Y chromosome haplotype is determined accordingly. Figure 4B shows a composite of electrochemical data obtained from five hybridizations with different individual samples. The results demonstrate that the ADNC can be used to distinguish target haplotypes in a system involving a mixture of heterogeneous and relatively long sequences.

The ANDC-based DNA detection approach offers several unparalleled features. First, its basic properties are independent of medium of substrates, indicators, and detection systems, which make it compatible with many conventional materials and methods. Other approaches, such as electrochemical methods or labeling methods, are highly dependent on specific mediator or detection apparatus (33,34), and cannot allow compatibility with each other. Second, conventional systems based on labeling methods (34) increase target selectivity by changing the hybridization temperature to a stringent range (usually <5°C). In this system, it is feasible in a broad temperature range (∼30°C). One obtains better discrimination of matches and mismatches without changes in temperature. Third, it is not necessary to label targets or probes. This feature simplifies the protocol for DNA chips, possibly reducing its cost compared to those labeling-based methods. Finally, the mechanical properties of ADNC greatly enhance the discrimination of matches and mismatches on simple conditions, unlike many other methods that enhance the discrimination by the addition of more procedures (salt washing, silver enhancing, etc.).

Triple-state ADNC

One extra improvement on ADNC is using DNA hairpin-loop (35–37) as motif unit, which results in a triple-state ADNC. When the DNA loop was zipped by itself, the nanocompartment is formed with small room, which is named s-on state. When the DNA loop hybridized with 'fuel' strands, the nanocompartment is formed with large room (38), which is named l-on state. The three states illustrated in Figure 5B can be distinguished from their encaging isotherms (Figure 5A). Operation on ADNC is determined by the stability of each state, which is affected by the following factors: temperature (15), ionic strength of hybridization buffer (11,15) and presence or absence of competing strands complementary to 'fuel' strands. For a dual-state ADNC, cyclic switching can be achieved by changing the factors mentioned above. For a triple-state ADNC, the stability of each state can be controlled via modulation of ionic strength and temperature (35–37). Figure 5C shows cyclic switching of the triple-state ADNC between two combinatorial states following these operation principles. In the absence of both external 'fuel' strands and ionic strength, the off state is stable in operation solution >25°C. In absence of external 'fuel' strands and the presence of 1 mM Mg^{2+}, the s-on state is stable <54°C. In the presence of both external 'fuel' strands and 1 mM Mg^{2+}, the l-on state is stable <42°C.

Another improvement may be the use of appropriate electric field control to accelerate the determination of ADNC states (39). However, an investigation of how the electric potential would change the encaging effect is a nontrivial task, and it is therefore reserved for future studies. In addition, the reasons for the ADNC being switchable is worthy of study in future research, which may involve the cooperativity mechanism in formation of the duplex monolayer (40).

CONCLUSION

This study demonstrates the reversible control of switching for DNA nanocompartments on surfaces. We show that a generality of DNA nanocompartment and its core property is invariant, relative to the changes of specific substrate, selected indicator, and hybridization protocols. It is reasonable that

its unique functions come from its dynamic nanostructure. While other researchers demonstrated surface switching for a low-density monolayer in wetting behavior (10), this study exhibits an alternative approach to reversibly switching surfaces with respect to molecular mechanical behavior, which shows possible applications in electrochemical energy storage, thermal molecule sensing, drug release, and nucleic acid analysis. Our results suggest that DNA nanocompartments could be used as building blocks for complex nanosystems, and that it promises to be integrated with the microfabrication and microfluidic technology to enable future biomaterial research (41).

SUPPLEMENTARY MATERIAL

Supplementary Material is available at NAR Online.

ACKNOWLEDGEMENTS

We thank T. P. Zhao, Y. Q. Zhan and Z. G. Wang for helping in preparation of Au(111) and X. Li for preparing supplementary documents. This work was partly supported by the Ministry of Science and Technology of China and the research fund from Peking University.

REFERENCES

1. Mao,C., Sun,W., Shen,Z. and Seeman,N.C. (1999) A nanomechanical device based on the B-Z transition of DNA. *Nature*, **397**, 144–146.
2. Yuke,B., Turberfield,A.J., Mills,A.P.Jr, Simmel,F.C. and Neumann,J.L. (2000) A DNA-fueled molecular machine made of DNA. *Nature*, **406**, 605–608.
3. Yan,H., Zhang,X., Shen,Z. and Seeman,N.C. (2002) A robust DNA mechanical device controlled by hybridization topology. *Nature*, **415**, 62–65.
4. Braun,E., Eichen,Y., Sivan,U. and Ben-Yoseph,G. (1998) DNA-templated assembly and electrode attachment of a conducting silver wire. *Nature*, **391**, 776–778.
5. Kasumov,A.Y. Kociak,M., Gueron,S., Reulet,B., Volkov,V.T., Klinov,D.V.and Bouchiat,H. (2001) Proximity-induced superconductivity in DNA. *Science*, **291**, 280–282.
6. Benenson,Y., Paz-Elizur,T., Adar,R., Keinan,E., Livneh,Z. and Shapiro,E. (2001) Programmable and autonomous computing machine made of biomolecules. *Nature*, **414**, 430–434.
7. Winfree,E., Liu,F., Wenzler,L.A. and Seeman,N.C. (1998) Design and self-assembly of two-dimensional DNA crystals. *Nature*, **394**, 539–544.
8. Park,S.J., Taton,A. and Mirkin,C.A. (2002) Array-based electrical detection of DNA with nanoparticle probes. *Science*, **295**, 1503–1506.
9. Gittins,D.I., Bethell,D., Schiffrin,D.J. and Nichols,R.J. (2000) A nanometer-scale electronic switch consisting of a metal cluster and redox-addressable groups. *Nature*, **408**, 67–69.
10. Lahann,J., Mitragotri,S., Tran,T.N., Kaido,H., Sundaram,J., Choi,I.S., Hoffer,S., Somorjai,G.A. and Langer,R. (2003) A reversibly switching surface. *Science*, **299**, 371–374.
11. Steel,A.B., Herne,T.M. and Tarlov,M.J. (1998) Electrochemical quantitation of DNA immobilized on gold. *Anal. Chem.*, **70**, 4670–4677.
12. Herne,T.M. and Tarlov,M.J. (1997) Characterization of DNA probes immobilized on gold surfaces. *J. Am. Chem. Soc.*, **119**, 8916–8920.
13. Kelley,S.O., Barton,J.K., Jackson,N.M., McPherson,L.D., Potter,A.B., Spain,E.M., Allen,M.J. and Hill,M.G. (1998) Orienting DNA helices on gold using applied electric fields. *Langmuir*, **14**, 6781–6784.
14. Kelley,S.O. and Barton,K.B. (1997) Electrochemistry of methylene blue bound to a DNA-modified electrode. *Bioconjug. Chem.*, **8**, 31–37.
15. Okahata,Y., Kawase,M., Niikura,K., Ohtake,F., Furusawa,H. and Ebara,Y. (1998) Kinetic measurements of DNA hybridization on an oligonucleotide-immobilized 27-MHz quartz crystal microbalance. *Anal. Chem.*, **70**, 1288–1296.
16. Yang,M., Yau,H.C.M. and Chan,H.L. (1998) Adsorption kinetics and ligand-binding properties of thiol-modified double-stranded DNA on a gold surface. *Langmuir*, **14**, 6121–6129.
17. Guo,Z., Guilfoyle,R.A., Thiel,A.J., Wang,R. and Smith,L.M. (1994) Direct fluorescence analysis of genetic polymorphisms by hybridization with oligonucleotide arrays on glass supports. *Nucleic Acids Res.*, **22**, 5456–5465.
18. Paraschiv,V., Zapotoczny,S., de Jong,M.R., Vancso,G.J., Huskens,J. and Reinhoudt,R.N. (2002) Functional group transfer from gold nanoparticles to flat gold surfaces for the creation of molecular anchoring points on surfaces. *Adv. Mater.*, **14**, 722–726.
19. Jing,T.W., Jeffrey,A.M., DeRose,J.A., Lyubchenko,Y.L., Shlyakhtenko,L.S., Harrington,R.E., Appella,E., Larsen,J., Vaught,A. and Rekesh,D. (1993) Structure of hydrated oligonucleotides studied by *in situ* scanning tunneling microscopy. *Proc. Natl Acad. Sci. USA*, **90**, 8934–8938.
20. Allemand,J.F., Bensimon,D., Lavery,R. and Croquette,V. (1998) Stretched and overwound DNA forms a Pauling-like structure with exposed bases. *Proc. Natl Acad. Sci. USA*, **95**, 14152–14157.
21. Giese,B. Amaudrut,J., Kohler,A.K., Spormann,M. and Wessely,S. (2001) Direct observation of hole transfer through DNA by hopping between adenine bases and by tunnelling. *Nature*, **412**, 318–320.
22. Lewis,F.D., Wu,T., Zhang,Y., Letsinger,R.L., Greenfield,S.R. and Wasielewski,M.R. (1997) Distance-dependent electron transfer in DNA hairpins. *Science*, **277**, 673–676.
23. Bard,A.J. and Fulkner,L.R. (1980) *Electrochemical methods*. Wiley, New York, NY.
24. Pease,A.C., Solas,D., Sullivan,E.J., Cronin,M.T., Holmes,C.P. and Fodor,S.P. (1994) Light-generated oligonucleotide arrays for rapid DNA sequence analysis. *Proc. Natl Acad. Sci. USA*, **91**, 5022–5026.
25. Tuite,E. and Nordén,B. (1994) Sequence-specific interactions of methylene blue with polynucleotide and DNA: a spectroscopic study. *J. Am. Chem. Soc.*, **116**, 7548–7556.
26. Rohs,R., Sklenar,H., Lavery,R. and Roder,B. (2000) Methylene blue binding to DNA with alternating GC base sequence: a modeling study. *J. Am. Chem. Soc.*, **122**, 2860–2866.
27. Ohuigin,C., McConnell,D.J., Kelly,J.M. and van der Putten,W.J. (1987) Methylene blue photosensitized strand cleavage of DNA: effects of dye binding and oxygen. *Nucleic Acids Res.*, **15**, 7411–7427.
28. Aoki,H., Buhlmann,P. and Umezawa,Y. (2000) Electrochemical detection of a one-base mismatch in an olgionucleotide using ion-channel sensors with self-assembled PNA monolayers. *Electroanalysis*, **12**, 1272–1276.
29. Cater,M.T., Rodriguez,M. and Bard,A.J. (1989) Voltammetric studies of the interaction of metal chelates with DNA. 2. Tris-chelated complexes of cobalt(III) and iron(II) with 1,10-phenathroline and 2,2′-bipyridine. *J. Am. Chem. Soc.*, **111**, 8901–8911.
30. Johnston,D.H. and Thorp,H.H. (1996) Cyclic voltammetry studies of polynucleotide binding and oxidation by metal complexes: homogeneous electron-transfer kinetics. *J. Phys. Chem.*, **100**, 13837–13843.
31. Underhill,P.A.Shen,P., Lin,A.A., Jin,L., Passarino,G., Yang,W.H., Kauffman,E., Bonne-Tamir,B., Bertranpetit,J., Francalacci,P. *et al.* (2000) Y chromosome sequence variation and the history of human populations. *Nature Genet.*, **26**, 358–361.
32. Underhill,P.A., Passarino,G., Lin,A.A., Shen,P., Mirazon Lahr,M., Foley,R.A., Oefner,P.J. and Cavalli-Sforza,L.L. (2001) The phylogeography of Y chromosome binary haplotypes and the origins of modern human populations. *Ann. Hum. Genet.*, **65**, 43–62.
33. Boon,E.M., Ceres,D.M., Drummond,T.G., Hill,M.G. and Barton,J.K. (1996) Mutation detection by electrocatalysis at DNA-modified electrodes. *Nat. Biotechnol.*, **14**, 303–308.

34. Taton,T.A., Mirkin,C.A. and Letsinger,R.L. (2000) Scanometric DNA array detection with nanoparticle probes. *Science*, **289**, 1757–1763.
35. Tyagi,S. and Kramer,F.R. (1996) Molecular beacons: probes that fluoresce upon hybridization. *Nat. Biotechnol.*, **14**, 303–308.
36. Bonnet,G., Tyagi,S., Libchaber,A. and Kramer,F.R. (1999) Thermodynamic basis of the enhanced specificity of structured DNA probes. *Proc. Natl Acad. Sci. USA*, **96**, 6171–6176.
37. Bonnet,G., Krichevsky,O. and Libchaber,A. (1998) Kinetics of conformational fluctuations in DNA hairpin-loops. *Proc. Natl Acad. Sci. USA*, **95**, 8602–8606.
38. Mao,Y., Luo,C. and Ouyang,Q. (2003) Studies of temperature-dependent electronic transduction on DNA hairpin loop sensor. *Nucleic Acids Res.*, **31**, e108.
39. Sosnowski,R.G., Tu,E., Butler,W.F., O'Connell,J.P. and Heller,M.J. (1997) Rapid determination of single base mismatch mutations in DNA hybrids by direct electric field control. *Proc. Natl Acad. Sci. USA*, **94**, 1119–1123.
40. Jin,R.Wu.G., Li,Z., Mirkin,C.A. and Schatz,G.C. (2003) What controls the melting properties of DNA-linked gold nanoparticle assemblies. *J. Am. Chem. Soc.*, **125**, 1643–1654.
41. Cheng,J. and Kricka,L.J. (2001) *Biochip Technology*. Harwood Academic Publishers, Philadelphia, PA.